LULEÅ UNIVERSITY OF TECHNOLOGY

2002:244 CIV

MASTER'S THESIS

# Design and Analysis of an Electrically Steerable Microstrip Antenna for Ground to Air Use

Johan Lagerqvist

**MASTER OF SCIENCE PROGRAMME**

Department of Computer Science and Electrical Engineering
Division of EMC center

2002:244 CIV • ISSN: 1402 - 1617 • ISRN: LTU - EX - - 02/244 - - SE

# Design and Analysis of an Electrically Steerable Microstrip Antenna for Ground to Air Use

Johan Lagerqvist

May 2002

# Chapter 1

# Abstract

A single-feed circularly polarized microstrip antenna array, operating at 2.45 GHz, have been analyzed and designed. The antenna is mainly intended to be used for reception of a video signal transmitted from an unmanned aircraft, but can be used for other applications as well. Due to the fact that it is supposed to be used in a switched system, the beam width is quite narrow. Measurements of the antenna shows that it have a half power beam width of 40°. For a VSWR lower than 1.5 and an axial ratio lower than 3 dB the bandwidth is 80 MHz centered at 2.44 GHz. The side lobe levels are less than −23 dB.

The antenna is designed to be simple in layout due to the fact that it should be as robust as possible against manufacturing faults.

# Chapter 2

# Acknowledgements

I wish to thank my advisor Stewart Jenvey for the time he spent with me, not only for the project but also for various other matters that did not concern this thesis. I would also like to thank Ray Chapman for the etching of the antenna and Ian Reynolds for his computer support. Without his help I would have spent more time messing with the computer than working.

Finally I would like to thank Australian Telecommunications Cooperative Research Centre (ATcrc) for funding my stay in Australia and Taconic Advanced Dielectric Division for being generous and supplying the substrate used for the antenna for free.

# Contents

# List of Figures

# Chapter 3

# Introduction

## 3.1 Thesis Motivation

In a joint research project, Monash University and Aerosonde Ltd are developing an unmanned aircraft with a video camera. The video signal is transmitted to ground control, at a frequency of 2.45 GHz, where it can be analyzed in real time. The aircraft is intended to be used for various missions, such as weather observations and "search and rescue" operations.

Currently, the signal is transmitted, and received, using a dipole antenna which, due to its nature is linearly polarized. Thus, when the receiving and transmitting antennas are not aligned in parallel to each other, energy will be lost between them. This is the case when the aircraft is turning and thus banking.

Another major problem with the current design is that the the frequency that the video signal is transmitted on, 2.45 GHz, belongs to a licence free band. Since it is a free band there might be one, or several, transmitters within range that the receiving antenna can pick up.

The purpose of this master thesis is to redesign the ground antenna, that receive the video signal from the aircraft, in order to improve reception.

In parallel with this thesis, there are two other ongoing theses [3][4] closely related to this thesis. The main purposes of the other two theses are to redesign the aircraft mounted transmitting antenna and to analyze the data received from the redesigned ground based receiving antenna.

## 3.2 Design Specifications

As mentioned above, there are two main reasons for why the current transmitter/reciever system has to be redesigned. First the current system uses linear polarization and secondly, since the ground stationed receiving antenna currently is a dipole antenna, all transmitters working at 2.45 GHz, within range, will be picked up by the receiving antenna.

In order to avoid energy loss as a result of two misaligned linearly polarized antennas, it has been decided that both the transmitting and receiving antenna should be circularly polarized.

Since there are no practical reasons for why either right hand circular polarization (RHCP) or left hand circular polarization should be chosen, RHCP was arbitrary chosen.

To prevent the ground station from picking up an interfering transmission at the same frequency, the radiation pattern from the receiving antenna should be dynamic, ie. it should be possible to modify the radiation pattern, so that the interfering transmitter can be blocked out without affecting the reception from the aeroplane.

The antenna should be reasonable easy to move around. This, so the positioning of the ground antenna is not the limiting factor to where the plane can be used. Due to the above requirement it has been decided that a microstrip antenna should be used. The microstrip antenna also have the advantage that the feed network can be incorporated into the antenna design, thus making it even more mobile.

Finally, the bandwidth of the radio frequency (RF) signal transmitted from the aircraft is 15 MHz and thus this is the lowest acceptable bandwidth for the receiving antenna. Within the bandwidth the VSWR should be lower than 1.5 and the axial ratio should be lower than 3 dB.

A secondary goal, if time permits, is to design the receiving antenna so that it in conjunction with receiving the video signal, it can also operate as a monopulse radar that can track the aerosonde.

## 3.3 Literature Review

Mankind's strive for effective communication is perhaps one of the reasons for why we distinguish ourself from the rest of the animals on this earth. Development have gone from sound and visual signals to today's use of electromagnetism to transfer information. For this antennas are used.

For an explanation of the laws of electromagnetism, [5] is recommended reading. There are several books describing antenna fundamentals, of which [1] and [6] are two excellent sources of information.

Microstrip antennas is probably the, in recent time, most investigated antenna due to properties like light weight, thin and the possibility of integrating the feed network into the antenna design. Due to the fact that it is a fast evolving research area, most information about microstrip antennas can be found in articles. However there are some good books available, for example [7] and [2], where the former is a handbook, that despite being old, still covers many aspects of microstrip antennas. [2] focuses on the design of microstrip antennas with the help of computers.

Some good review articles are [8], [9], [10] and [11], where the first three mainly cover single element microstrip antennas and the last one covers array technology for microstrip antennas. They are all quite old, but despite that they still give a good introduction to the advantages, and disadvantages, of microstrip antennas.

## 3.4 Thesis Overview

The first part of the second chapter covers the theory behind linearly and circularly polarized microstrip antennas and techniques used to build the network for a microstrip array. The second part covers how it is possible to steer an antenna electrically, ie without any mechanical parts. Finally a simple technique for tracking the aircraft is presented.

Chapter three describes the design of an microstrip antenna array, discussing aspects like the size of the array, which type of element should be chosen and substrate selection. In the end of the chapter measurements of the antenna are presented.

Finally, conclusions and recommendations for future work are presented in chapter four.

# Chapter 4

# Background Theory

## 4.1 Microstrip Antennas

As can be seen in Figure 4.1, a microstrip patch antenna is built up in a similar way to a parallel plate capacitor. Both have two metal layers and a dielectric material in between the two metal layers. In a microstrip patch antenna, the lower conducting layer is called ground plane, the dielectric material, substrate and finally the top conducting layer, patch. The size of this patch depends of the wavelength and thus the microstrip patch antenna is classified as a resonant antenna. As with all resonant antennas, the bandwidth is narrow, usually only a few percent[12].

### 4.1.1 Linearly Polarized Microstrip Antennas

Figure 4.1 shows a patch antenna, in which the patch is rectangular and it is thus called rectangular patch antenna. When feed, a standing wave will occur as shown in Figure 4.2, but some of the field will "leak out" around the edges of the patch. This is the so called fringing field. In the figure, we can see that the electric field on the left side outside the patch is going into the patch and on the other side leaving the patch[1].

A real valued output impedance is desired and this requires that the antenna operates at resonance. In order for the antenna to operate at resonance the length, L, is usually set to slightly less than half a wavelength in

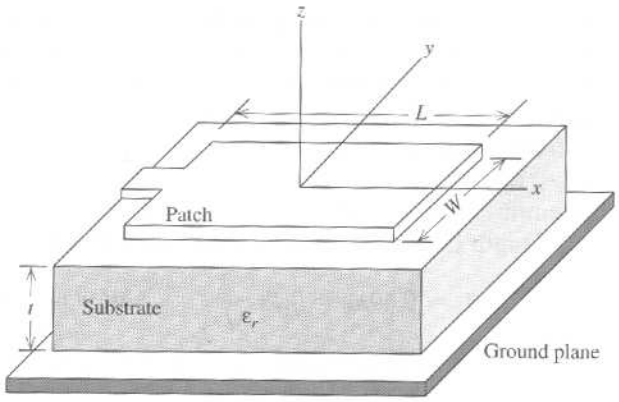


Figure 4.1: The geometry of a typical microstrip patch antenna. Picture from [1].

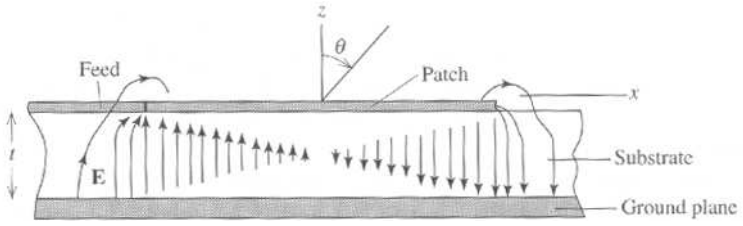


Figure 4.2: Side view of a microstrip patch antenna, showing the electric fields. Picture from [1].

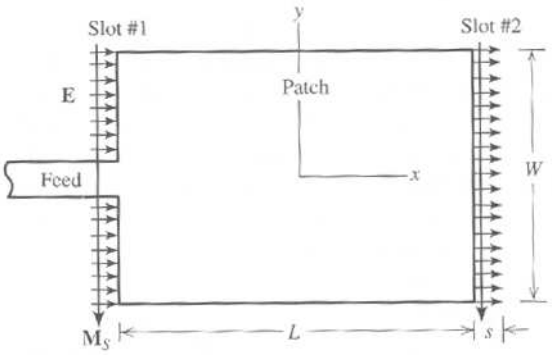


Figure 4.3: Two radiating slots used to model a microstrip patch antenna. Picture from [1].

the dielectric material, ie

$$L = 0.49\frac{\lambda}{\epsilon_r}. \tag{4.1}$$

The reason for why it is not set exactly to half a wavelength is that the fringing fields will be located just outside the patch[1].

Looking from the top, down at the patch, the electric fields are pointing in the same direction, ie they are in phase. From above this will look like two rectangular radiating areas and can thus be approximated by two radiating slots, both in phase. The thicker the substrate is, the more the electric field will "leak out" around the edges of the patch and thus the approximating slots should be made wider. For a thickness of the substrate, t, much less than a wavelength, the width of the slot is assumed to be equal to the thickness of the substrate[1]. This model is shown in Figure 4.3.

In order to calculate the radiation pattern from the patch antenna, we first calculate the radiation field from one of the approximating slots, after that we can use array theory to calculate radiation pattern from both slots.

Let $E_a$ be the, assumed constant, electric field over one of the slots shown in Figure 4.3. This electric field can be replaced with a magnetic current, $M_s$. According to Love's equivalence principle[5] the magnetic current is given by

$$M_s = E_a \times \hat{n}. \tag{4.2}$$

The electric vector potential, $F$, for a given magnetic current is

$$F = \epsilon \frac{e^{-j\beta r}}{4\pi r} \iint_S M_s(r') e^{j\beta \hat{r}\cdot r'} dS'. \tag{4.3}$$

Using (4.2) in (4.3), we get that

$$F = \epsilon \frac{e^{-j\beta r}}{4\pi r} \hat{n} \times \iint_{S_a} E_a e^{j\beta \hat{r}\cdot r'} dS', \tag{4.4}$$

where $S_a$ is the surface of the slot.

Looking in Figure 4.3, we see that the electric field is oriented along the x-axis, ie $E_a = E_0\hat{x}$, where $E_0$ is the magnitude of the electric field. Using this together with (4.4) and the fact that $\hat{n} = \hat{z}$, the electric vector potential can be written as

$$F = \epsilon \frac{e^{-j\beta r}}{4\pi r} \hat{z} \times \iint_{S_a} E_0 \hat{z} e^{j\beta \hat{r}\cdot r'} dS' = \hat{y} E_0 \epsilon \frac{e^{-j\beta r}}{4\pi r} \iint_{S_a} e^{j\beta \hat{r}\cdot r'} dS'. \tag{4.5}$$

The best coordinate system to express the slot surface with, is the cartesian. In this system, $r' = x'\hat{x} + y'\hat{y}$. Further it is most common to express the radiation pattern in spherical coordinates, ie $\hat{r} = \hat{x}\sin\Theta\sin\Phi + \hat{y}\sin\Theta\sin\Phi + \hat{z}\cos\Theta$. Performing these two transformations in (4.5) yields

$$F = \hat{y} E_0 \epsilon \frac{e^{-j\beta r}}{4\pi r} \iint e^{j\beta(x'\sin\Theta\cos\Phi + y'\sin\Theta\sin\Phi)} dS'. \tag{4.6}$$

Further, according to Figure 4.3, the limits of the integrals can be inserted, which gives that

$$\begin{aligned} F &= \hat{y} E_0 \epsilon \frac{e^{-j\beta r}}{4\pi r} \int_{-W/2}^{W/2} \int_{-s/2}^{s/2} e^{j\beta(x'\sin\Theta\cos\Phi + y'\sin\Theta\sin\Phi)} dx' dy' = \\ &= \hat{y} E_0 \epsilon \frac{e^{-j\beta r}}{4\pi r} W s \frac{\sin(\frac{\beta s}{2}u)}{\frac{\beta s}{2}u} \frac{\sin(\frac{\beta W}{2}v)}{\frac{\beta W}{2}v}, \end{aligned} \tag{4.7}$$

where $u \equiv \sin\Theta\cos\Phi$ and $v \equiv \sin\Theta\sin\Phi$. As stated above, the length of the slot can approximately be set equal to the thickness of the dielectric material when the thickness is much less than a wavelength. If this is the case we can use that[13]

$$\lim_{x\to 0} \frac{\sin x}{x} = 1 \tag{4.8}$$

and get that

$$F = \hat{y} E_0 W s \epsilon \frac{e^{-j\beta r}}{4\pi r} \frac{\sin(\frac{\beta W}{2} v)}{\frac{\beta W}{2} v}. \tag{4.9}$$

Further using that[1]

$$\hat{y} = \hat{r} \sin\Theta \sin\Phi + \hat{\Theta} \cos\Theta \sin\Phi + \hat{\Phi} \cos\Phi, \tag{4.10}$$

it is possible to retrieve the theta and phi components from (4.9),

$$F_\Theta = \cos\Theta \sin\Phi E_0 \epsilon \frac{e^{-j\beta r}}{4\pi r} W s \frac{\sin(\frac{\beta W}{2}) v}{\frac{\beta W}{2} v} \tag{4.11}$$

$$F_\Phi = \cos\Phi E_0 \epsilon \frac{e^{-j\beta r}}{4\pi r} W s \frac{\sin(\frac{\beta W}{2}) v}{\frac{\beta W}{2} v}. \tag{4.12}$$

The far zone magnetic field associated with the electric vector potential is given by[1]

$$H_F = -j\omega(F_\Theta \hat{\Theta} + F_\Phi \hat{\Phi}). \tag{4.13}$$

Note that the index $F$ in $H_F$ above means that it is the magnetic field associated with the electric vector potential ($F$) and that it is the sum of the magnetic field associated with the electric vector potential and magnetic field associated with the magnetic vector potential that gives the total magnetic field.

In the far field, the EM wave can be approximated as plane, thus

$$E_F = \eta H_F \times \hat{r} = -j\omega\eta(F_\Phi \hat{\Phi} - F_\Theta \hat{\Phi}). \tag{4.14}$$

Inserting 4.11 and 4.12 into 4.14 we get

$$E_F = -j\epsilon\omega\eta E_0 \frac{e^{-j\beta r}}{4\pi r} W s \frac{\sin(\frac{\beta W}{2} v)}{\frac{\beta W}{2} v} (\cos\Phi \hat{\Theta} - \cos\Theta \sin\Phi \hat{\Phi}). \tag{4.15}$$

The ground plane can be assumed to be a perfect electric conductor. When this is the case an equivalent problem can be created by mirroring the electric and magnetic currents in the xy-plane[5]. When an electric current is mirrored, the direction of it has to be inverted. Since the patch is assumed to be very close to the ground plane, this means that the image will cancel out the real electric current. A magnetic current that is mirrored is not inverted

and thus the magnetic current in the new problem will be twice that of the original problem. Thus the magnetic vector potential does not have to be calculated. This result in that the total electric field will be

$$E = 2E_F = -j\epsilon\omega\eta E_0 \frac{e^{-j\beta r}}{2\pi r} W s \frac{\sin(\frac{\beta W}{2} v)}{\frac{\beta W}{2} v} (\cos\Phi\hat{\Theta} - \cos\Theta\sin\Phi\hat{\Phi}). \quad (4.16)$$

From this we get that the normalized principle plane far field patterns are

$$g_E(\Theta) = 1 \quad (4.17)$$

$$g_H(\Theta) = \cos\Theta \frac{\sin(\frac{\beta W}{2}\sin\Theta)}{\frac{\beta W}{2}\sin\Theta}, \quad (4.18)$$

where $g_E$ is the E-plane pattern ($\Phi = 0$) and $g_H$ is the H-plane pattern ($\Phi = 90°$).

Now we have been able to derive an expression for the radiation pattern in the principle planes for one slot. In order to determine the radiation pattern for both slots, we first calculate the radiation pattern for the case when the slots are replaced by two isotropic point sources located in the center of the slots that they replace[1]. The H-plane is located right between the two elements. This results in that any point in the H-plane always will have the same distance to both elements and the energy received at all points will be doubled. However, since the radiation pattern is normalized, there will be no difference in the H-plane radiation pattern for one compared with two elements.

Figure 4.4 shows a cut along the E-plane. Here we can see that an incoming plane wave will be picked up by the elements with a phase difference. Looking at the geometry it can be noted that the element to the right will be $\frac{L}{2}\sin\Theta$ in front of a fictitious element located in the origin. In the same way, the left element will lag the fictitious element with the same amount. Inserting this into the expression for the radiation field for a isotropic antenna, $\frac{e^{-\beta r}}{4\pi r}$, and using superposition we get that the total radiation pattern for both elements, in the E-plane, is

$$AF_E = e^{-j\beta\frac{L}{2}\sin\Theta} + e^{j\beta\frac{L}{2}\sin\Theta} = 2\cos(\frac{\beta L}{2}\sin\Theta), \quad (4.19)$$

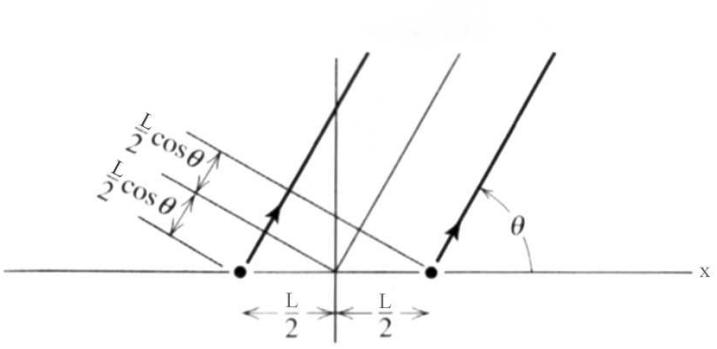


Figure 4.4: A cut in the xz-plane of a two element array. Figure from [1], slightly modified for our coordinate system.

where $AF_E$ stands for the Array Factor in the E-plane and tells us how identical antennas that are pointing in the same direction interfere with each other. If we normalize this we get that the normalized array factor is

$$f_E(\Theta) = \cos(\frac{\pi}{2}\sin\Theta) \tag{4.20}$$

The total pattern for the two slits can be calculated by multiplying the array factor with the element factor. Thus the total pattern for the E-plane will be

$$\begin{aligned} F_E(\Theta) &= g_E(\Theta)f_E(\Theta) = \\ &= \cos(\frac{\beta L}{2}\sin\Theta) \end{aligned} \tag{4.21}$$

and for the H-plane

$$\begin{aligned} F_H(\Theta) &= g_H(\Theta)f_H(\Theta) = \\ &= \cos\Theta\frac{\sin(\frac{\beta W}{2}\sin\Theta)}{\frac{\beta W}{2}\sin\Theta}. \end{aligned} \tag{4.22}$$

Using "a rigorous Sommerfeld solution" it has been shown that the approximative output impedance is

$$Z_A = 90\frac{\epsilon_r^2}{\epsilon_r - 1}(\frac{L}{W})^2 \tag{4.23}$$

and that the bandwidth, $B$, approximately is

$$B = 3.77\frac{\epsilon_r - 1}{\epsilon_r^2}\frac{t}{\lambda} \tag{4.24}$$

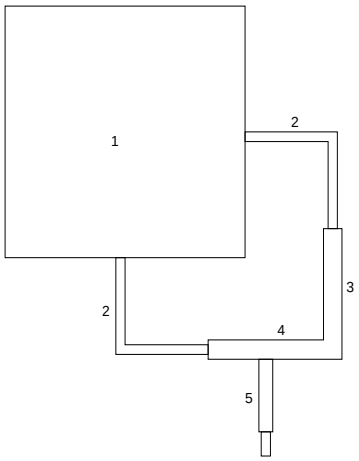


Figure 4.5: A dual feed circularly polarized microstrip patch antenna.

for the square patch[14].

### 4.1.2 Circularly Polarized Microstrip Antennas

In order to achieve circular polarization, two orthogonal standing waves, 90° out of phase compared to each other, are required in the microstrip antenna[2].

The easiest way of achieving this, from the point of understanding, is to feed a square patch on two adjacent sides, where one of the feeds is delayed 90°. One possible design, using this method, is shown in Figure 4.5. Here we can see that the antenna consists of five different parts. First we have the actual square patch (1). Connected to the patch are two $\lambda/4$-transformers (2). The purpose of these are to transform the usually high output impedance from the patch to an impedance level that it is possible to design a microstrip transmission line for[2].

After the $\lambda/4$-transformer to the right, we have a 90° phase shifter (3). In order to simplify the T-junction, the lower $\lambda/4$-transformer is followed by microstrip line designed for the new lower impedance. The 90° phase shifter is followed by a similar transmission line. These two transmission lines are merged together in a T-junction (4) to a new $\lambda/4$-transformer (5). When

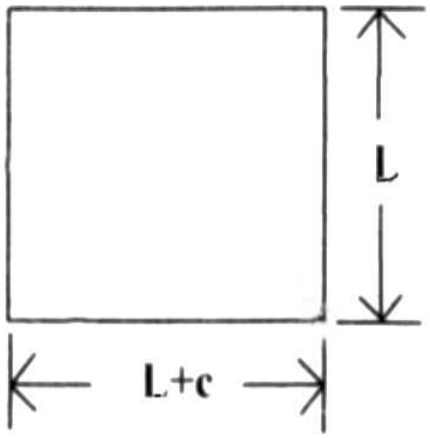


Figure 4.6: A circularly polarized nearly square microstrip patch antenna. Picture from [2].

the two transmission lines are merged together, the new impedance will be half that of the impedance of each of the transmission lines. That is why the new $\lambda/4$-transformer is there, to prevent that the outgoing transmission line gets too low impedance and thus gets to wide. Finally, the $\lambda/4$-transformer is attached to the feed.

The disadvantage of using two feed points to a single patch in order to get circular polarization is the complexity. As described above, there are many parts required to make it work. Instead it would be better if the patch itself would induce circular polarization.

One common way of achieving this is by having a nearly square patch that is feed on its diagonal[7], as shown in Figure 4.6. If a square patch is feed on its diagonal two orthogonal modes with equal amplitude will be created, due to the symmetry of the problem. However there will not be a $90^\circ$ phase difference between the two modes. That is why one of the sides of the patch is made slightly longer. When this is done the resonance frequencies will differ slightly between the two modes. By correctly choosing the extra length of the side, it is possible to make this slight difference in frequency cause the $90^\circ$ phase difference[2].

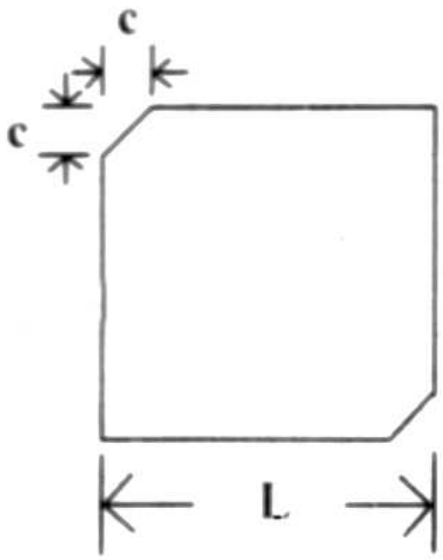


Figure 4.7: A circularly polarized truncated corner microstrip patch antenna. Picture from [2].

Another similar way of achieving circular polarization from a single feed patch is to feed the patch on one of the sides and truncate the corners of a square patch[7], as shown in Figure 4.7. If the corners were not truncated, one resonance mode will occur from the the side that is feed to the opposite side. This would create linear polarization as described in previous section. When the corners are truncated, the resonance will not occur from one side to the other side, but along the diagonals[2]. Since one of the diagonals is shorter than the other, the resonance frequencies will differ slightly for the two modes. If the corners are truncated exactly the right amount, the difference in frequencies will cause the 90° phase shift, exactly in the same way as for the nearly square path.

The main difference between the truncated square patch and the nearly square patch is that the truncated patch have a lower output impedance compared to the nearly square patch. This, since the truncated patch is feed on its side and not along its diagonal, as the case is for the nearly square patch[7]. For this reason the truncated square patch will be used for this

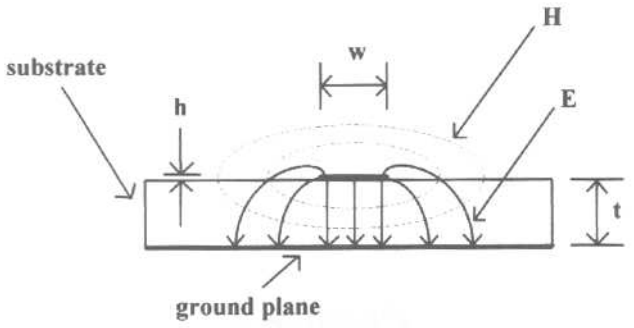


Figure 4.8: Cross section of a microstrip transmission line showing the electric fields. Picture from [2].

project.

There are methods for calculating the extra length of the near square patch and the size of the truncated corners of the truncated patch given in [7], but with the introduction of computers it is usually more convenient to find out the extra length or the size of the truncated segment with computer simulations instead. That is the method used throughout this report.

### 4.1.3 Microstrip Discontinuities

The cross section of a microstrip transmission line is shown in Figure 4.8. As can be seen in this figure, the electric fields on each side of the strip line are pointing in the exactly opposite direction[2]. Thus, as long as the width, w, is much shorter than a wavelength the electric fields will cancel out each other and no radiation will occur. However, a straight transmission line is very uncommon, usually it is bent in some places, transmission lines are joined together in intersections, etc. These 'additions' to the microstrip lines are called microstrip discontinuities.

There are mainly two microstrip discontinuities that will be used in this report, the microstrip bend and the T-junction. Both are shown in Figure 4.9.

For most applications the microstrip bend is the most common discontinuity. In the bend, the electric current density will be higher on the inside of the bend then on the outside. This will make the radiation fields on each

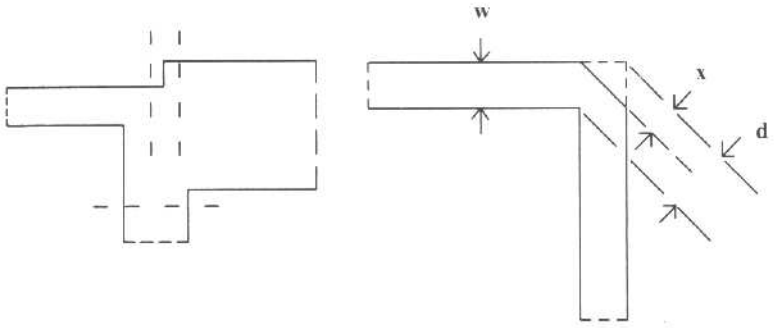


Figure 4.9: Two microstrip discontinuities, the T-junction and the microstrip bend. Picture from [2].

side of the transmission line different from each other and thus the bend will radiate[2].

It has been shown that this radiation can be eliminated by chamfering the bend as illustrated in Figure 4.9. The optimum size of the chamfering has been determined to[2]

$$\frac{x}{d} = 0.52 + 0.65e^{-1.35\frac{w}{t}}, \tag{4.25}$$

where w is the width of the transmission line, t is the thickness of the dielectric substrate and $\frac{x}{d}$ is the ratio that the corner should be chamfered for optimum result, as shown in Figure 4.9. When this is done, the electrical length through the bend will be shorter. Compared to the distance along the center line, the reduction will be[2]

$$\frac{\Delta b}{D} = 0.16(2 - (\frac{f}{f_p})^2), \tag{4.26}$$

where $D = \frac{\eta_0 t}{\sqrt{\epsilon_r} Z_0}$ and $f_p(GHz) = 0.4\frac{Z_0}{h}(mm)$. $Z_0$ is the impedance of the transmission line and $\eta_0$ is the free space intrinsic impedance, defined as $\eta_0 = \sqrt{\mu_0/\epsilon_0}$.

When a transmission line is split, a T-junction is used as shown in Figure 4.9. The only split used in this report is the equal power split, ie both the branches will receive half of the input power. The power input is

$$P_{in} = \frac{1}{2}\frac{V_0^2}{Z_0}. \tag{4.27}$$

Assume that $P_1$ and $P_2$ are the output power, then

$$P_1 = P_2 = \frac{1}{2}\frac{V_0^2}{Z_{out}} = \frac{1}{2}P_{in}, \tag{4.28}$$

since an equal power split is desired. $Z_{out}$ is the impedance of the output transmission lines. Inserting (4.27) into (4.28), we get that

$$Z_{out} = 2Z_{in}. \tag{4.29}$$

The impedance, $Z_0$, is given by[2]

$$Z_0 = \frac{\eta_0}{2\pi\sqrt{\epsilon_{re}}} \ln\left(\frac{8t}{W_e} + 0.25\frac{W_e}{t}\right) \qquad \text{for } \frac{W}{t} \leq 1 \tag{4.30}$$

$$Z_0 = \frac{\eta_0}{\sqrt{\epsilon_{re}}} \left[\frac{W_e}{t} + 1.393 + 0.667 \ln\left(\frac{W_e}{t} + 1.444\right)\right]^{-1} \qquad \text{for } \frac{W}{t} \geq 1 \tag{4.31}$$

where

$$\frac{W_e}{t} = \frac{W}{t} + \frac{1.25}{\pi}\frac{h}{t}\left[1 + \ln\left(\frac{4\pi W}{h}\right)\right] \qquad \text{for } \frac{W}{t} \leq \frac{1}{2\pi} \tag{4.32}$$

$$\frac{W_e}{t} = \frac{W}{t} + \frac{1.25}{\pi}\frac{h}{t}\left[1 + \ln\left(\frac{2t}{h}\right)\right] \qquad \text{for } \frac{W}{t} \geq \frac{1}{2\pi} \tag{4.33}$$

and

$$\epsilon_{re} = \frac{\epsilon_r + 1}{2}\frac{\epsilon_r - 1}{2} F\left(\frac{W}{t}\right) - C \tag{4.34}$$

and

$$F\left(\frac{W}{t}\right) = \left(1 + 12\frac{t}{W}\right)^{-1/2} + 0.04\left(1 - \frac{W}{t}\right)^2 \qquad \text{for } \frac{W}{t} \leq 1 \tag{4.35}$$

$$F\left(\frac{W}{t}\right) = \left(1 + 12\frac{t}{W}\right)^{-1/2} \qquad \text{for } \frac{W}{t} \geq 1 \tag{4.36}$$

$$C = \frac{\epsilon_r - 1}{4.6}\frac{\frac{h}{t}}{\sqrt{\frac{W}{t}}}. \tag{4.37}$$

These equations can only be used when the dispersion is so small that it can be ignored.

As described above, in the microstrip bend the current will take a 'short cut' through the bend and thus the electrical length will be shorter than the

length along the center line. This will also be the case for the T-junction. Throughout this report this reduction in electrical length is calculated using a MS-DOS program, mictee.exe that is available at http://www.ece.mcmaster.ca/faculty/georgieva/antennas_files/sainati/. Here it is also possible to find a program, micmiter.exe, which calculates the desired chamfering for a given microstrip bend, using the equations mentioned above.

## 4.2 Smart Antennas

"A smart antenna system combines multiple antenna elements with a signal-processing capability to optimize its radiation and/or reception pattern automatically in response to the signal environment"[15]. There are several possible designs that can produce this. For this project two different methods will be analyzed, phased arrays and switched antennas.

### 4.2.1 Phased Arrays

Using the same technique as in Section 4.1.1, it is possible to derive the array factor for a two dimensional rectangular array as[1]

$$AF(\Theta,\Phi) = \sum_{n=1}^{N}\sum_{m=1}^{M} I_{mn} e^{j\alpha_{mn}} e^{j\xi_{mn}} \tag{4.38}$$

where

$$\xi_{mn} = \beta\hat{r}\cdot\hat{r}'_{mn} = \beta(x'_{mn}\sin\Theta\cos\Phi + y'_{mn}\sin\Theta\sin\Phi) \tag{4.39}$$

$$\alpha_{mn} = -\beta(x'_{mn}\sin\Theta_0\cos\Phi_0 + y'_{mn}\sin\Theta_0\sin\Phi_0) \tag{4.40}$$

and $\Theta_0$ and $\Phi_0$ gives the direction of the main beam. $I_{mn}$ and $\alpha_{mn}$ is the amplitude and phase of element $mn$. Thus by varying the the phase and amplitude of each individual element it is possible to synthesize the desired radiation pattern.

### 4.2.2 Switched Antennas

In the phased array, all elements are uniform and pointing in the same direction while interference is used to control the radiation pattern. Another

possible smart antenna design would be to design the elements to be directive and point them in different directions. Then the radiation pattern can be controlled by switching between the elements. The radiation pattern is built up of several main lobes and by correctly choosing the element, the desired signal can be received without interference from the other directions.

## 4.3 Monopulse Tracking Radar

For a two-element, in phase, linear array with a spacing of half a wavelength, the array factor can be calculated from (4.38) as

$$AF_s = 1 + e^{j\pi \sin\Theta} \tag{4.41}$$

and for the same case, but when the two elements are 180° out of phase

$$AF_d = 1 - e^{j\pi \sin\Theta}. \tag{4.42}$$

These two patterns are called sum and difference patterns.

If this array was connected to a feed network that could synthesize both the sum and difference pattern, the transmission could be received using the sum pattern and by analyzing the differences in sum and difference pattern the angle between the direction of the transmitter and the normal of the array plane, $\Theta$, can be calculated.

The energy received decreases with the square of the distance from the transmitter and receiver, but for the quotient of the sum and difference pattern this range dependant will be cancelled out. Using equation (4.41) and (4.42) the absolute value of this quotient can be written as

$$\begin{aligned}
\left|\frac{AF_d}{AF_s}\right| &= \left|\frac{1 - e^{j\pi \sin\Theta}}{1 + e^{j\pi \sin\Theta}}\right| = \left|\frac{e^{-j\frac{\pi}{2}\sin\Theta} - e^{j\frac{\pi}{2}\sin\Theta}}{e^{-j\frac{\pi}{2}\sin\Theta} + e^{j\frac{\pi}{2}\sin\Theta}}\right| = \\
&= \left|-\frac{2j\sin\left(\frac{\pi}{2}\sin\Theta\right)}{2\cos\left(\frac{\pi}{2}\sin\Theta\right)}\right| = \left|-j\tan\left(\frac{\pi}{2}\sin\Theta\right)\right| = \\
&= \left|\tan\left(\frac{\pi}{2}\sin\Theta\right)\right|
\end{aligned} \tag{4.43}$$

Looking at this quotient, it is only possible to decide the absolute value of the angle, since the function is symmetric. However, the phase difference

between the sum and difference pattern is

$$\arg\left(AF_s\right) - \arg\left(AF_d\right) = \arg\left(1 + e^{j\pi\sin\Theta}\right) - \arg\left(1 - e^{j\pi\sin\Theta}\right) \tag{4.44}$$

$$= \arg\left(\frac{1 + e^{j\pi\sin\Theta}}{1 - e^{j\pi\sin\Theta}}\right) = \arg\left(\frac{e^{-j\frac{\pi}{2}\sin\Theta} + e^{j\frac{\pi}{2}\sin\Theta}}{e^{-j\frac{\pi}{2}\sin\Theta} - e^{j\frac{\pi}{2}\sin\Theta}}\right) \tag{4.45}$$

$$= \arg\left(-\frac{2\cos\left(\frac{\pi}{2}\sin\Theta\right)}{2j\sin\left(\frac{\pi}{2}\sin\Theta\right)}\right) = \arg\left(j\cot\left(\frac{\pi}{2}\sin\Theta\right)\right) \tag{4.46}$$

$$= \begin{cases} \frac{\pi}{2} & 0 < \Theta < \frac{\pi}{2} \\ -\frac{\pi}{2} & \frac{\pi}{2} < \Theta < 0 \end{cases} \tag{4.47}$$

and thus it is possible to use a phase detector, for example [16], to decide the sign of the angle.

# Chapter 5

# Design and Analysis

## 5.1 Smart Antenna Design

As mentioned in Section 4.2, two different types of smart antennas systems will be analyzed for this project. In order for the smart antenna to be able to correctly decide where the aerosond is located and direct the beam towards it, signal processing of the received signals from all the elements has to be done. The purpose of the Master's thesis [3], which is closely related to this thesis, is to do this analysis with a Digital Signal Processor(DSP).

Three different cases for the phased array were analyzed, all shown in Figure 5.1. In the top system, the RF signal from each element in the array is down converted to an intermediate frequency, which then is sampled by an A/D converter. A digital down converter (DDC) down converts the signal to base band and finally the base band signal is sent to the DSP. The intermediate frequency is used to "minimize the impact of variations in analog devices"[17]. In this method, the DSP has to be able to analyze information received at twice the base band frequency for each element in the array. The factor of two comes from the Nyqvist criteria. The base band frequency for the video transmission is approximately 7 MHz. For an array consisting of 16 elements, that would mean that 16 signals, each 14 Mhz, would have to be analyzed.

In the middle figure a Gain Phase Detector(GPD), for example [16], is used to measure the relative phase and amplitude of the RF signal between the elements. This information is analyzed by the DSP in order to decide

where the aerosond and possible interfering transmitters are. When this is known the DSP can synthesize the radiation pattern with the help of phase shifters and attenuators, in order to receive the video signal.

In the bottom figure, the signal from each element is modified by a phase shifter and an attenuator, added together and sampled into the DSP. By looking at the quality of the signal in to the DSP and changing the out signals to the phase shifters and attenuators, it is possible to solve this as a control system problem.

The final method analyzed is the case with a switched antenna. Here the signal from each element goes to a switch that is controlled by the DSP. After the switch the chosen signal is down converted to base band and sampled to the DSP.

Due to time constrains and cost, all systems but the switched antenna system was eliminated. The elimination process is described in detail in [3].

## 5.2 Array Layout

From (4.21) and (4.22) we get that the half power beam width for a square patch with side lengths equal to one half wavelength approximately is 60° for the E-plane and 120° in the H-plane for a linearly polarized patch. A circularly polarized antenna does not have E and H-planes, but it seems reasonable to assume that the half power beam width should be somewhere between the two calculated values above.

In order to increase the directivity of the antenna, an array of patches can be made. Using (4.38) and (4.21), the radiation pattern for a 2x2 array, feed in phase with a spacing of half a wavelength, is

$$F_{2E} = \left|\frac{AF}{4}\right| F_E = \frac{\left|1 + e^{j\pi \sin\Theta}\right|}{2} \cos\left(\frac{\pi}{2}\sin\Theta\right) \tag{5.1}$$

in the E-plane and (4.38) and (4.21) gives the radiation pattern in the H-plane as

$$F_{2H} = \left|\frac{AF}{4}\right| F_H = \frac{\left|1 + e^{j\pi \sin\Theta}\right|}{2} \cos\Theta \frac{\sin(\frac{\pi}{2}\sin\Theta)}{\frac{\pi}{2}\sin\Theta}. \tag{5.2}$$

From these two equations we get that the half power beam width is 43°

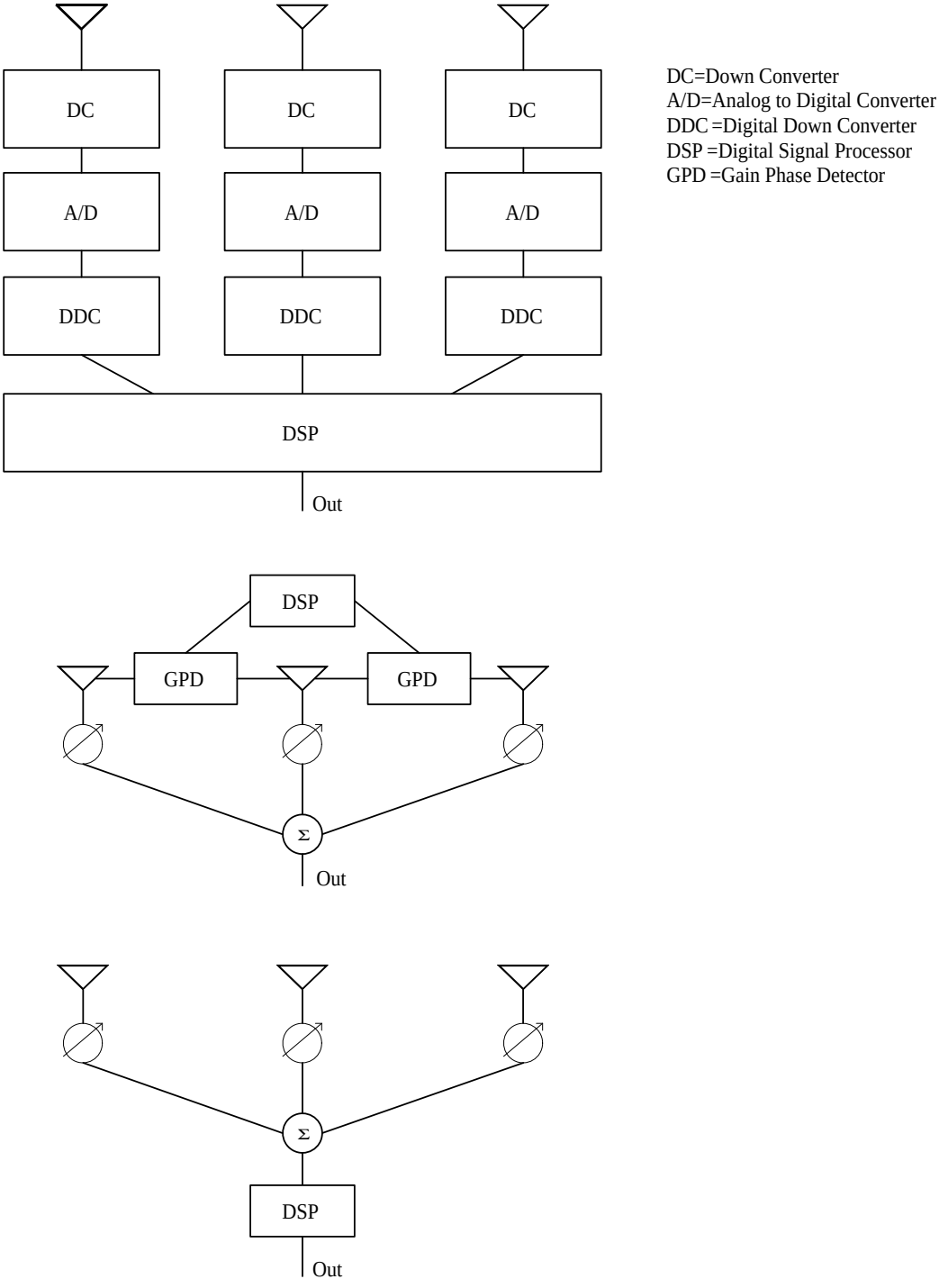


Figure 5.1: Three different possible implementations of a phased array.

in the E-plane and 46° in the H-plane. Similarly for a 3x3 array the half power beam width will be 32° in the E-plane and 33° in the H-plane.

As stated above, it seems reasonable that the half power beam width for the circularly polarized antenna should be close to these values.

Considering that the antenna gets bigger and bigger when the array size increases and thus will violate the design specification that specifies that the antenna has to be easy to move around, the size of the array have been chosen to 2x2, which is a good compromise between the size of the antenna and the directivity. The fact that it later should be possible to redesign the antenna for monopulse tracking also affects this choice. The number of elements on each side of the array has to be even for a monopulse tracking antenna.

## 5.3 Substrate Selection

The relative dielectric constant, $\epsilon_r$, will mainly affect the bandwidth (as shown in (4.24)), fabrication tolerance and the impedance of the patches and the transmission lines[2]. As can be seen in (4.1), the size of each patch is also affected by the dielectric constant.

The antenna will be built using a lithography machine available at Monash University. However this machine suffers from some minor defects that could make the final antenna not perfect. Due to this, as low dielectric constant as permitted by the size of the patches should be chosen.

In order to maximize the available space, and therefore allow a lower dielectric constant, the spacing between two elements have been chosen to $0.6\lambda$ and not $\lambda/2$ as used above when calculating the half power beam width. At 2.45 GHz, $0.6\lambda = 73.5$ mm.

This increased spacing will result in side lobes. Using the same technique as when calculating the half power beam width for the $\lambda/2$ case above the side lobe levels is calculated to -34 dB in the E-plane and -27 dB in the H-plane. The new half power beam width in the E-plane will be 39° in the E-plane and 41° in the H-plane. This analysis is based on that the ground plane is infinite. Since this for obvious reasons is not possible to build, the real antenna will have higher side lobe levels and a wider half power beam width

As stated above, the circularly polarized patch does not have E- and H-planes. In fact, the modes will not be oriented in the same direction. In the linearly polarized case, the mode will be parallel with one of the edges and for the truncated square patch the modes will be along its diagonals[7]. Despite this, it should still give a rough idea of the characteristics of the antenna.

The patches can not be located to close to each other due to mutual coupling. R. P. Jedlicka et al. in [18] have experimentally shown that if the distance from one edge of an element to the the closest edge of another element is greater than one quarter of a wavelength, mutual coupling can be ignored.

Assuming that the patches are squares with sides equal to half a wavelength in the dielectric material, the spacing between two elements are $0.6\lambda$ and the distance between two adjacent edges is $0.25\lambda$, we get that

$$0.6\lambda = 0.5\lambda_g + 0.25\lambda, \tag{5.3}$$

where $\lambda_g = \lambda/\sqrt{\epsilon_r}$ is the wavelength in the dielectric material. Solving for the relative dielectric constant we get that the lowest allowed relative dielectric constant is 2.04, ie $\epsilon_r \geq 2.04$.

A thicker substrate gives a higher bandwidth, as can be seen in (4.24) and better efficiency[2], but at the same time if the material is too thick surface waves might be excited. For a patch operating at a frequency, $f$, the thickness, $h$, of the substrate should satisfy[19]

$$h \leq \frac{0.3c}{2\pi f\sqrt{\epsilon_r}} \tag{5.4}$$

where $c$ is the speed of light in order to avoid surface waves.

Taconic Advanced Dielectric Division have generously supplied this project with one sheet (18"x24") of TLY-5A[20]. This material have a relative dielectric constant of 2.17 and the substrate is 1/8" = 3.175 mm thick. Each side of the substrate is coated with 35 $\mu m$ copper. The data sheet for the substrate is attached in Appendix A.

The maximum thickness, for avoiding surface waves, is according to (5.4) 3.96 mm for this material when operating at 2.45 GHz, thus surface waves should not be a problem.

## 5.4 Element Design

Ensemble 4.0 have been used to simulate a number of truncated square patches, varying the lengths of the sides and the size of the truncated corners.

Ensemble have a built in function that can estimate the layout of the truncated square patch with the help of "an approximate method based on the cavity model"[21]. This function recommends that the square length should be 39.73 mm and the corner length 5.65 mm if it is operating at 2.45 GHz, however this is only an approximative answer and should only be used as a guide line.

The main program in Ensemble simulates a given design and is based "on a full-wave approach using the mixed-potential integral equation formulation in conjunction with the method of moments"[21].

Considering that the program only can simulate a given design, the design procedure has to be trial and error with qualified guesses, using the approximative recommendation above as start design.

Simulating the truncated square patch with a square length 39.73 mm and the corner length 5.65 mm gives that the output impedance is 195Ω and the VSWR is below 1.45 within the band. The minimum value of the axial ratio is 1 dB at 2.44 GHz. Figure 5.2 shows the magnitude of the S-parameter, VSWR and axial ratio as a function of frequency for the simulation. The Smith chart is also shown there. Here we can see that it is the axial ratio, and not the VSWR, that limits the bandwidth. Considering this, some minor changes should be done in order to make sure that the axial ratio is minimized at 2.45 GHz.

With the current design, the axial ratio is at its minimum at 2.44 GHz and not 2.45 GHz, thus by making the antenna $(2.45 - 2.44)/2.44 = 0.41\%$ smaller the minimum value of the axial ratio would be moved to 2.45 GHz. With the new design the square length would be 39.57 mm and the corner length 5.63 mm.

Simulating this design gives that the output impedance is 196Ω and the results are shown in Figure 5.3. Here we see that the VSWR still is below 1.45 in the band and that the minimum value of the axial ratio now is at 2.45 GHz, but it is still at 1 dB and not zero, which is the optimum case.

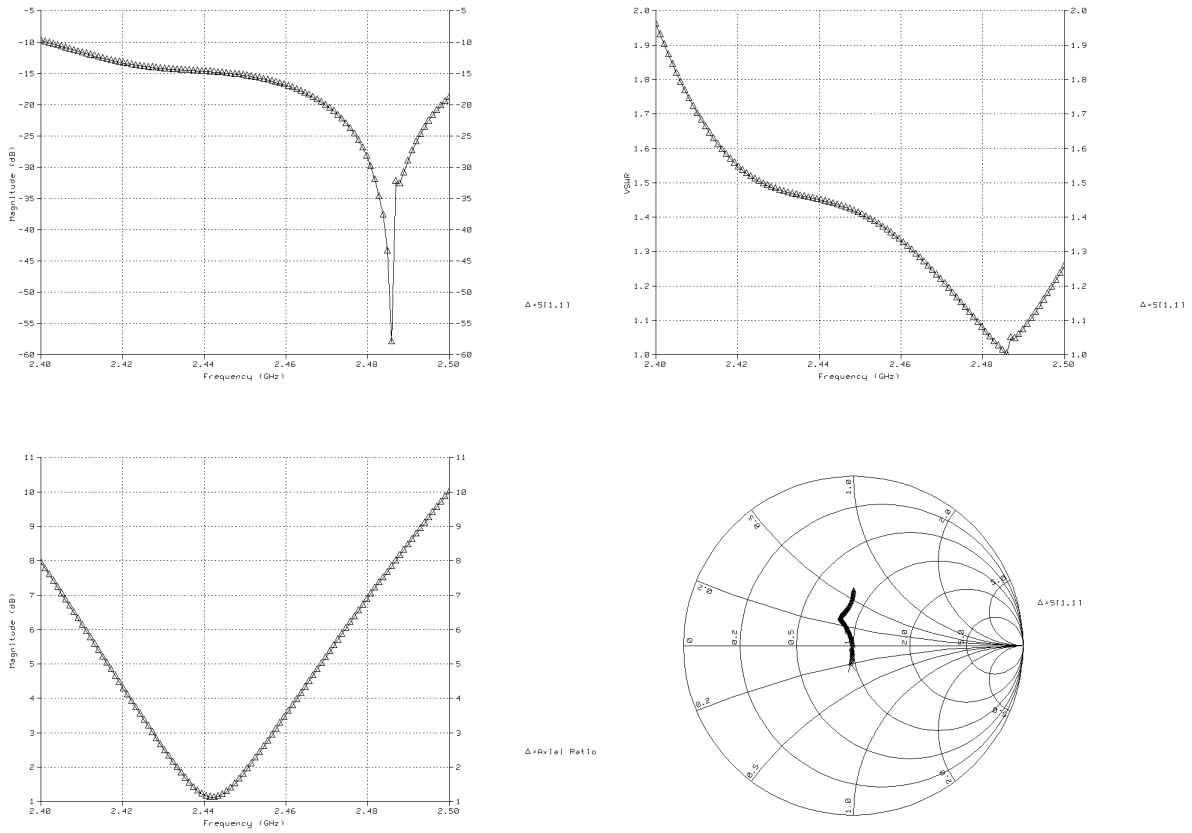


Figure 5.2: S-parameter, VSWR, Smith chart and axial ratio for a truncated square patch with square length 39.73 mm and corner length 5.65 mm.

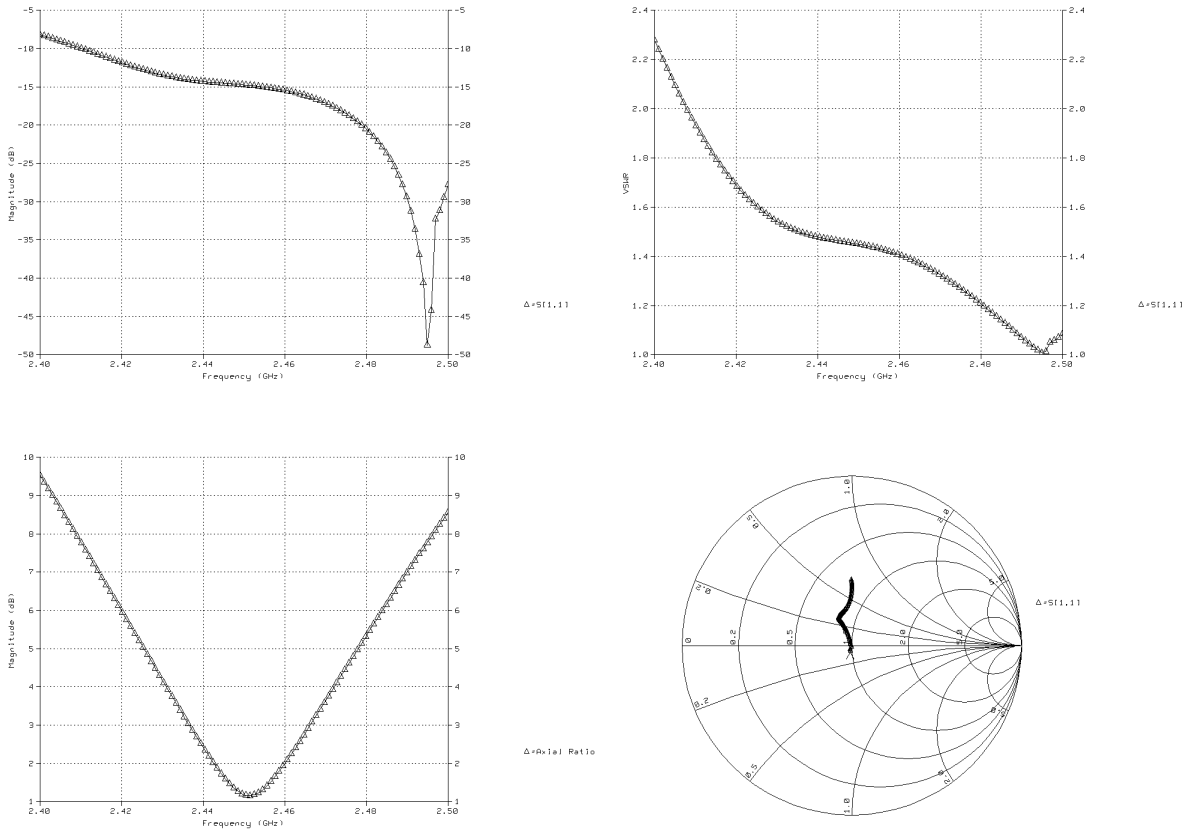


Figure 5.3: S-parameter, VSWR, Smith chart and axial ratio for a truncated square patch with square length 39.57 mm and corner length 5.63 mm.

Since it is the corner truncations that give rise to the circular polarization, the non optimal axial ratio means that the corner truncation is not optimal. Changing the corner length to 6 mm and maintaining the square length 39.57 mm will reduce the minimum value of the axial ratio to almost 0 dB. This change will also increase frequency where the optimum axial ratio is found to 2.455 GHz. The impedance is now 186Ω.

In order change to optimum frequency to 2.45 GHz, the square side length is changed to 39.67 mm. This results in a patch with an impedance of 190Ω. For an axial ratio of 3 dB or lower, the bandwidth is 35 MHz, centered at 2.45 GHz. Within this bandwidth, the VSWR is lower than 1.5. Detailed graphs are shown in Figure 5.4.

Figure 5.5 shows the final element design.

## 5.5 Array Design

In Section 5.2, it was decided that a 2x2 array should be used and in Section 5.3 the spacing was set to $0.6\lambda = 73.5$ mm.

The feed network is constructed by first connecting two adjacent elements together with a transmission line. The output impedance of each element is 190Ω, which corresponds to a 0.43 mm thick transmission line. This can be calculated from (4.30). From (4.25) we get that the 90° bend on the transmission line which is shown in Figure 5.6 should have a 0.455 mm truncated corner. Due to limitations in Ensemble, this truncation is set to 0.43 mm instead, ie the width of the transmission line. There is no need to compensate for the reduction in the electrical length of the transmission line due to the chamfering, since all four elements each have an equal bend and the relative phase is unaltered.

Now the two separate groups, each containing two elements, need to be connected together. This is done with a transmission line drawn between the centers of the 0.43 mm wide transmission lines. From (4.29) we get that the impedance of this transmission line should be $190/2 = 95\Omega$. (4.30) gives that the width should be 3.2 mm.

The array is feed by a probe in the middle of the thicker transmission line. Again using (4.29) we get that the probe ideally should have an impedance

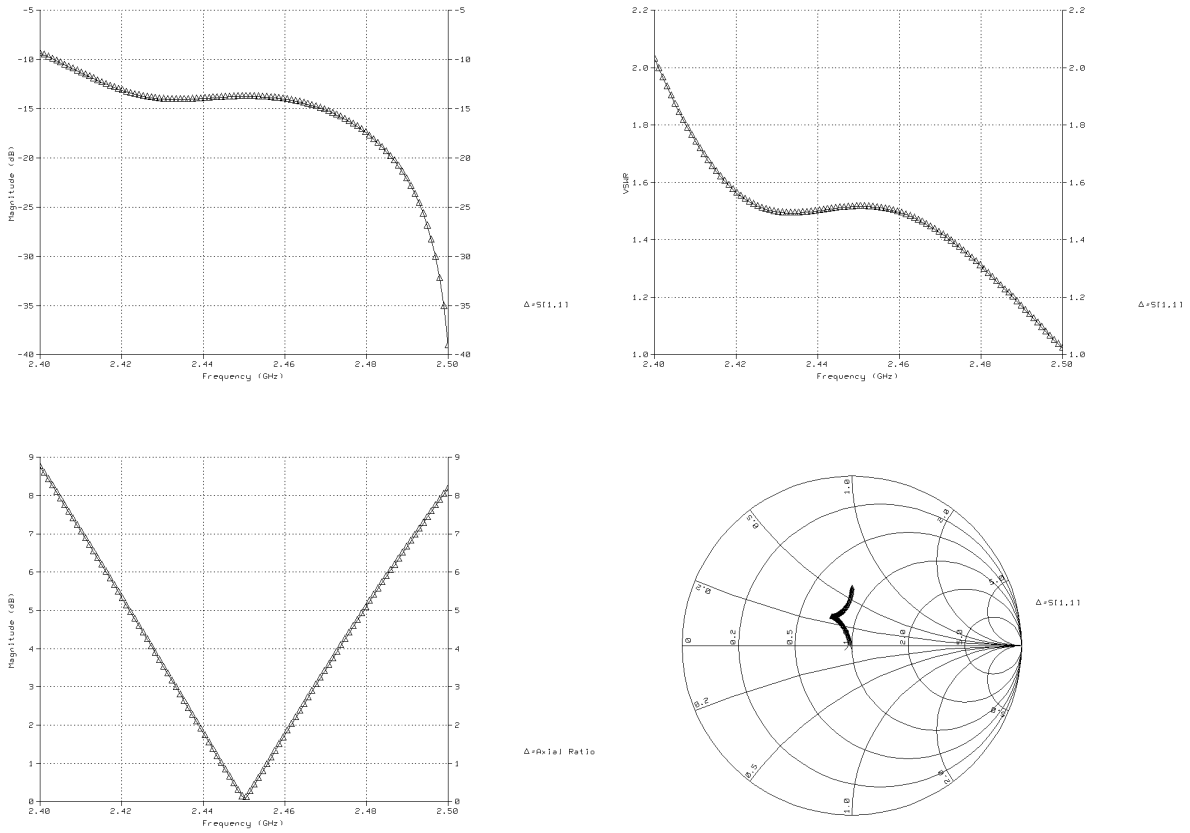


Figure 5.4: S-parameter, VSWR, Smith chart and axial ratio for a truncated square patch with square length 39.67 mm and corner length 6 mm.

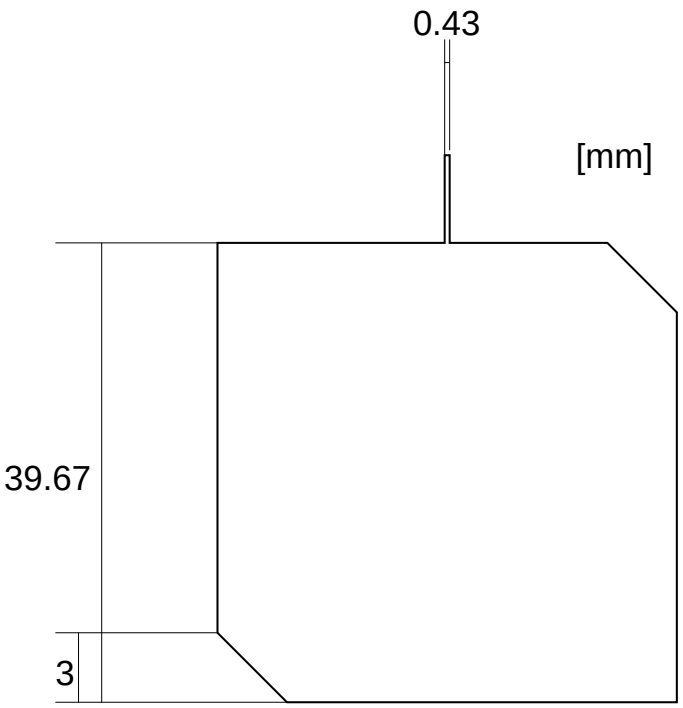


Figure 5.5: Final element design.

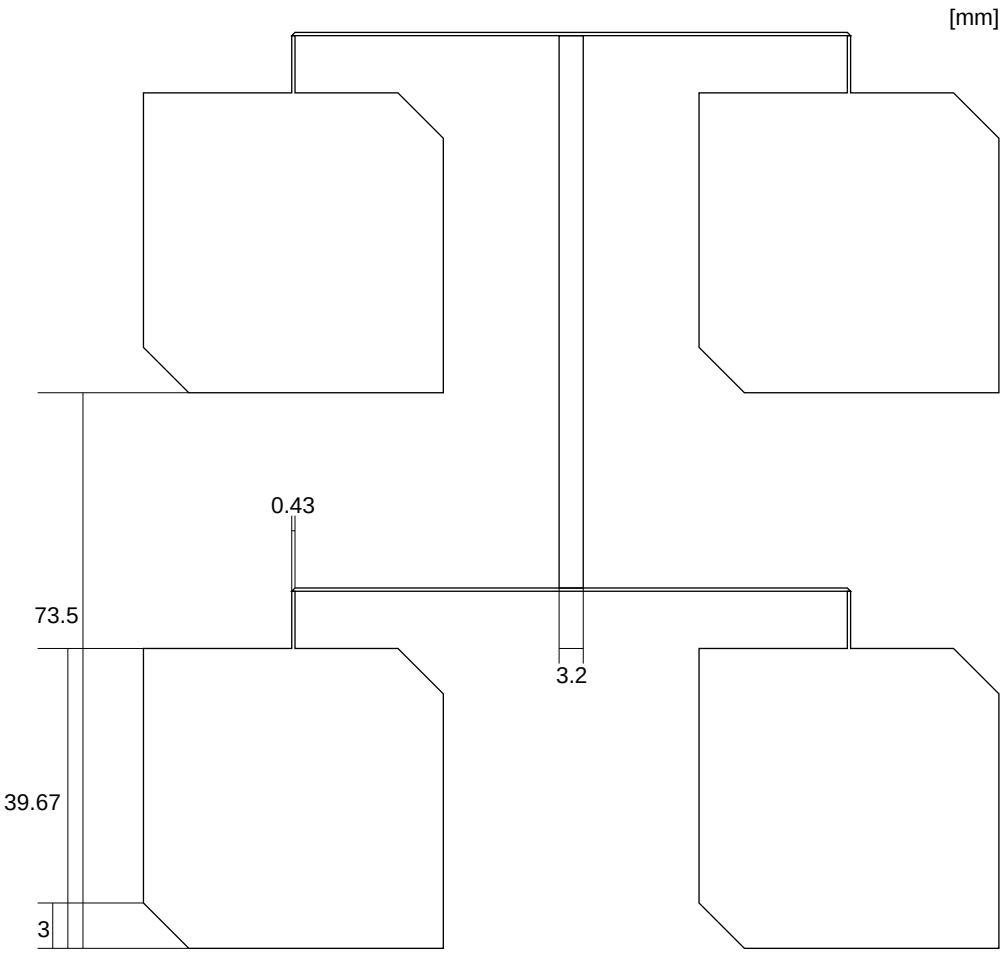


Figure 5.6: Geometry of a 2x2 circularly polarized microstrip antenna array.

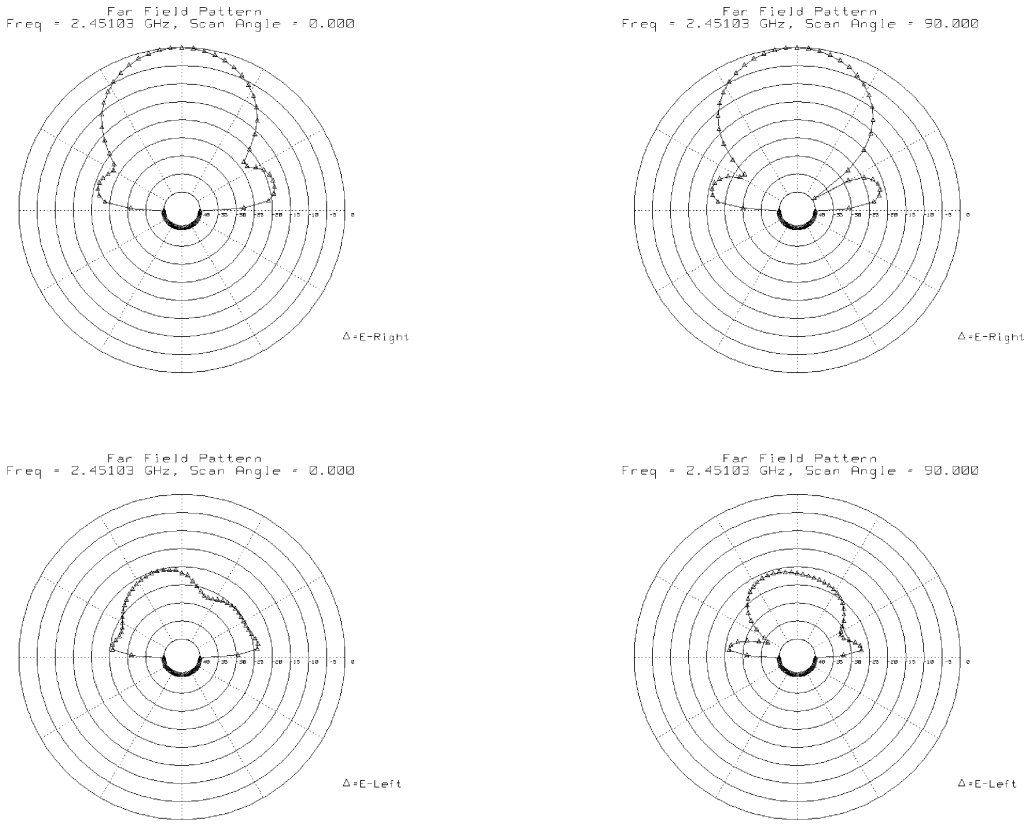


Figure 5.7: Radiation pattern for both right hand and left hand polarization for cuts in both principle planes of the antenna shown in Figure 5.6.

of $95/2 = 47.5\Omega$. Since a standard coaxial cable have an impedance of $50\Omega$ this is used instead.

Simulating this design with Ensemble gives that the 3 dB axial ratio bandwidth is 35 MHz centered at 2.46 GHz. Within the bandwidth, the VSWR is lower than 1.35. At 2.45 GHz, the side lobe levels are less than $-18$ dB, half power beam width of $50^\circ$ and a cross polarization less than $-20$ dB. Figures 5.7 and 5.8 shows the simulated radiation pattern and impedance characteristics for the antenna.

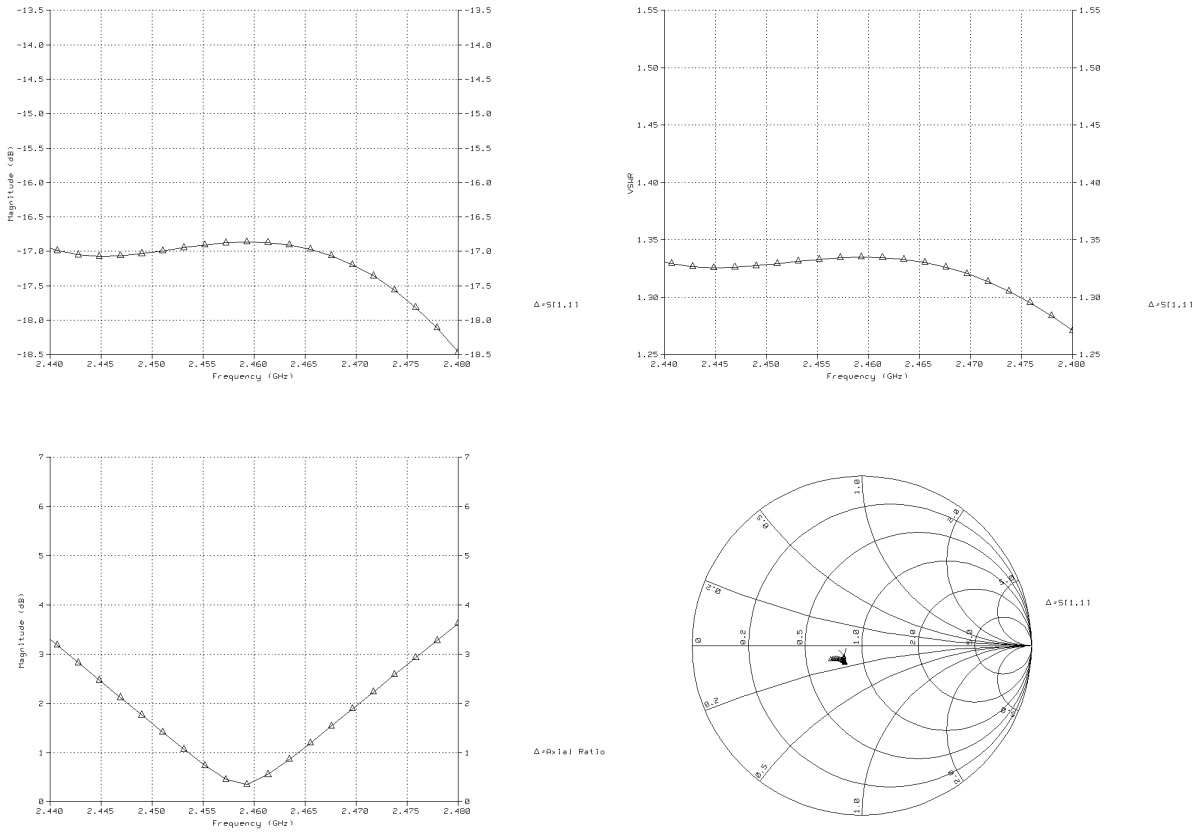


Figure 5.8: S-parameter, VSWR, Smith chart and axial ratio for the antenna shown in Figure 5.6.

## 5.6 Production

The design of Figure 5.6 was etched on to a laminate, TLY5-A as described in Section 5.3.

The larger the ground plane is, the closer the final antenna's characteristics will be to the computer simulation. In order to use as little dielectric material as possible and still have a large round plane, the design was etched on a substrate that was just slightly bigger (150 mm x 150 mm) then the antenna design itself. After that a copper sheet (in reality a cheap dielectric material coated with copper) with the dimensions 205 mm x 250 mm was attached on the side of the substrate that was not etched. Figure 5.9 shows a photo of the finished antenna.

## 5.7 Measurements

Monash University have an anechoic chamber that was used to measure the radiation characteristics of the antenna, but first the impedance of the antenna was measured using a network analyzer.

### 5.7.1 Impedance

In order to make sure that no radiation was received by the antenna during the impedance measurement the antenna was mounted inside the anechoic chamber, facing a wall. Considering that all walls of the chamber are coated with absorbing material almost all radiation from the outside should have been absorbed by the absorbers before it could have been received by the antenna.

After the antenna had been mounted, the network analyzer was connected using a 50Ω coaxial cable. Before the antenna was connected, the setup was calibrated for 50Ω. This was done in order to make sure that it is the impedance of the antenna and not the impedance of the antenna and the coaxial cable that is measured.

The results of the measurement are presented in Figure 5.10. Here it can be seen that the VSWR at 2.45 GHz is 1.45, which is not great, but fully acceptable considering that the design goal was to have a VSWR lower than

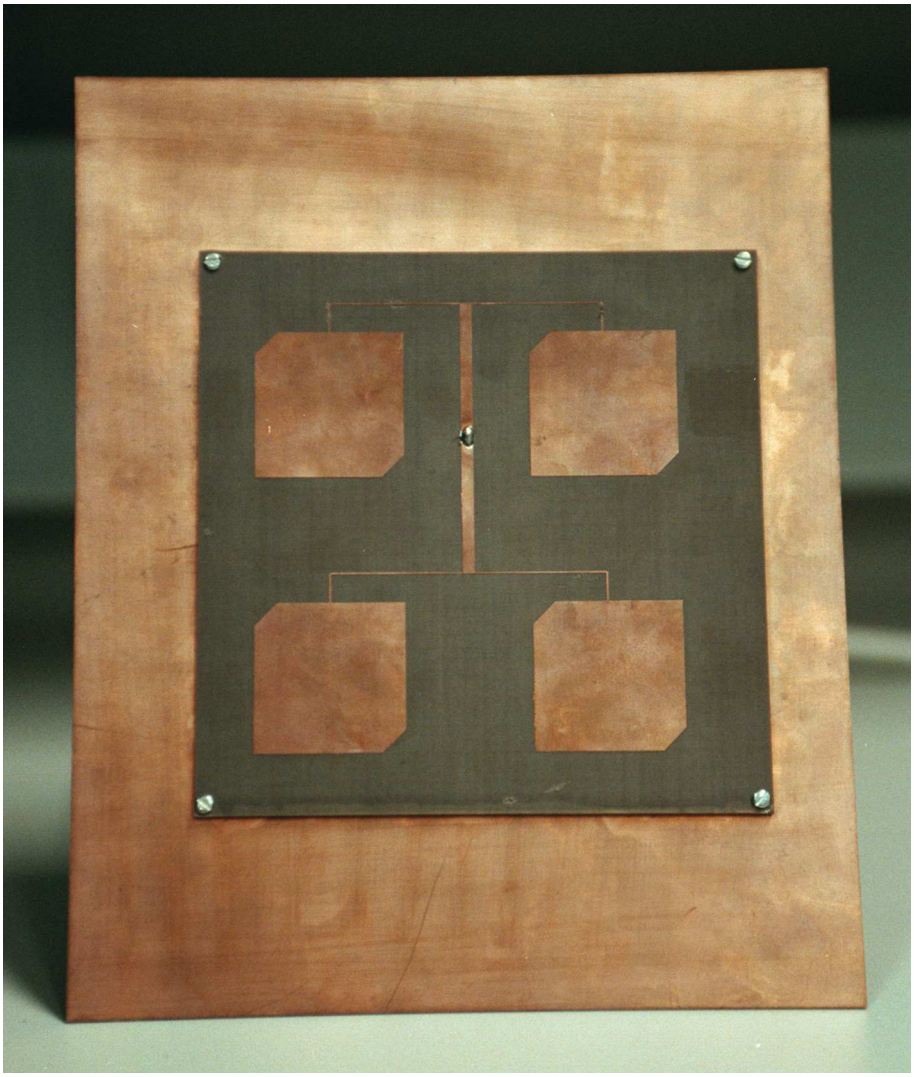

Figure 5.9: A photo of the finished antenna.

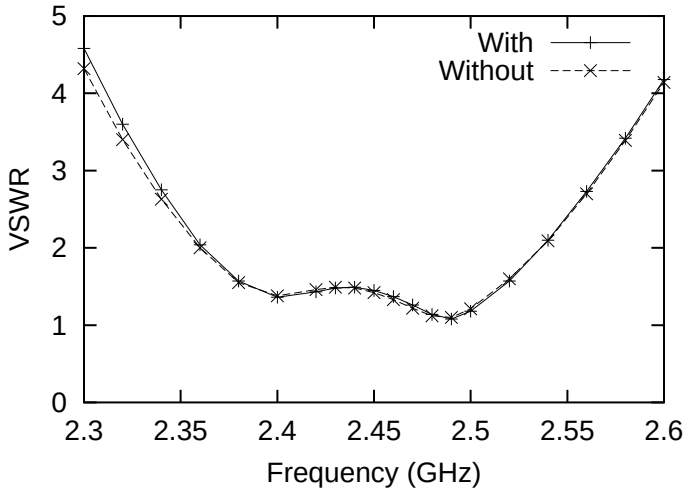


Figure 5.10: VSWR of the array in Figure 5.6 with and without the extra groundplane.

1.5. We can see that this design goal is fulfilled for frequencies from 2.39 GHz to 2.51 GHz, thus the bandwidth with respect to the VSWR is 120 MHz, centered at 2.45 GHz.

The same setup was used measuring the impedance of the antenna without the extra ground plane. The results from this measurement is given in Figure 5.10. We can see that the VSWR now is slightly less at 2.45 GHz, 1.42 compared to 1.45 in the previous measurement. The design goal for the VSWR gives exactly the same bandwidth as in the previous measurement, ie 120 MHz centered at 2.45 GHz. In reality the extra ground plane does not affect the impedance of the array.

### 5.7.2 Radiation pattern

Next the radiation pattern for the antenna was measured using a helical antenna, designed to operate at 2.45 GHz, as transmitting antenna and the patch antenna as receiver. Due to the symmetry of the helical antenna it will be right hand circularly polarized. No left hand circularly polarized antenna was available and thus the cross-polarization was not possible to measure.

In order to create the radiation pattern the patch was rotated 360°, measuring the amplitude of the received electric field for each degree. This was

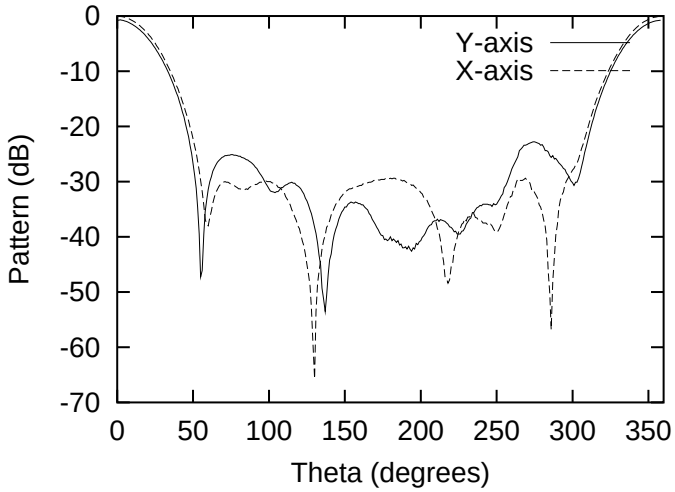


Figure 5.11: Radiation pattern for the array in Figure 5.6 operating at 2.45 GHz, where Theta is the angle rotated around X- or Y-axis.

later normalized in order to get the normalized radiation pattern. In Figure 5.11 the radiation pattern for rotation around both the x- and y-axis is presented.

Here we can see that the main lobe is orthogonal to the substrate, ie. the main lobe has not been scanned in any direction. This means that for maximum reception, the antenna should be aligned so that the etched side of the antenna is facing the transmitter. We can also see that the half power beam width is 40°. For rotation around the x-axis, the side lobe level is $-29$ dB and for rotation around the y-axis $-23$ dB.

In order to find the axial ratio, the same measurement was repeated twice with a linearly polarized horn antenna, instead of the helical antenna, oriented so the measured antenna would receive horizontal polarization in one measurement and vertical in the other. Due to time constrains the antenna was only rotated along its y-axis. This was done for a number of frequencies in order to be able to calculate the axial ratio as a function of the frequency and from this, calculate the bandwidth limitation due to the axial ratio.

A number of graphs showing the measured values for horizontal and vertical polarization can be found in Figure 5.12. From these graphs the axial ratio can be calculated as the absolute value of difference between the horizontally

polarized result and the vertically polarized in the main beam direction (0°). The axial ratio as a function of the frequency is plotted in Figure 5.13. From this graph we can see that the minimum value of the axial ratio (1.75 dB) is not at 2.45 GHz, but at 2.44 GHz. However it is still well below the design specification of 3 dB at 2.45 GHz. From the graph we can also see that the bandwidth with respect to the axial ratio is 80 MHz centered at 2.44 GHz.

In order to see how much the extra ground plane effects the radiation pattern, the radiation pattern was measured using the horn antenna without the extra ground plane mounted to the measured antenna. The results are plotted in Figure 5.14. We can see that the ground plane main effect is to reduce the side lobe levels. In the case with the ground plane the side lobes are less than $-23$ dB, while now without the extra ground plane they are lower than $-18$ dB.

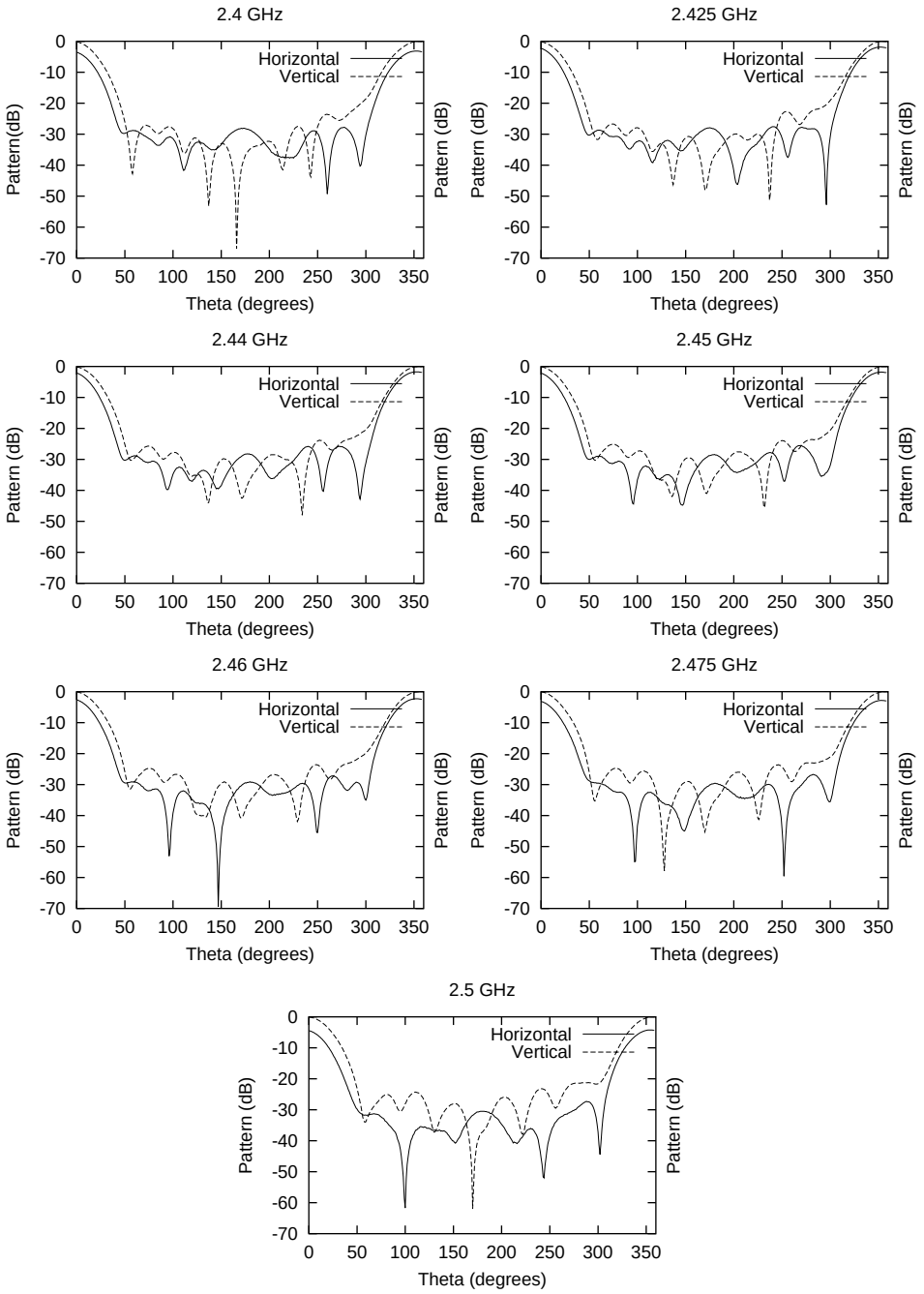


Figure 5.12: Horizontally and vertically polarized radiation pattern for the array in Figure 5.6 for various frequencies.

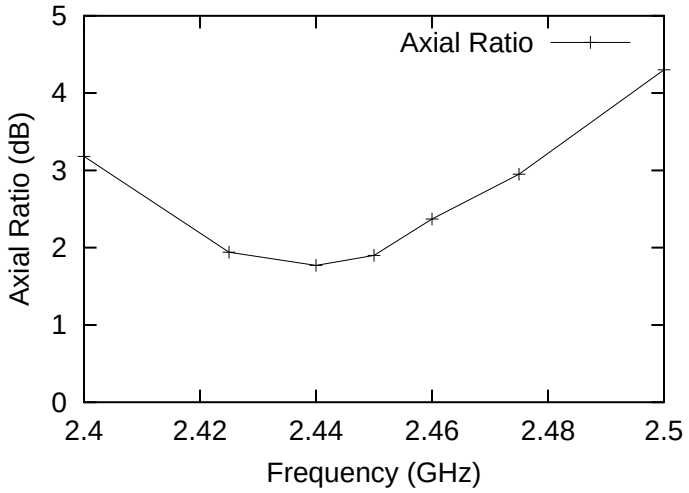


Figure 5.13: Axial ratio as a function of frequency for the array in Figure 5.6.

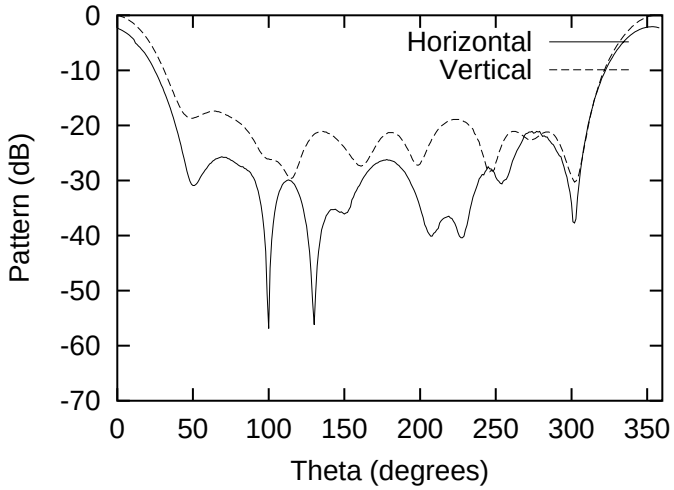


Figure 5.14: Horizontally and vertically polarized radiation pattern for the array in Figure 5.6 without the extra ground plane for 2.45 GHz.

# Chapter 6

# Conclusions

A circularly polarized microstrip patch antenna, designed for 2.45 GHz have successfully been built. Measurements show that the half power beam width is 40° and that for a VSWR lower than 1.5 and an axial ratio lower than 3 dB the band width is 80 MHz centered at 2.44 GHz.

Considering that the currently used system is based on linearly polarized transmission and the new design is based on circular polarization, there should be no problem with reduced or lost reception as a result of misaligned transmitting and receiving antennas, which the current system is suffering from.

When this patch antenna is used together with the switched antenna system designed in [3] the reception should be more robust against interfering transmission compared to the currently used system. Another advantage of using a switched system is that each element (ie. the antenna designed in this thesis) can have a higher directivity, compared to a non switched system, and still cover the same space. Higher directivity leads to that a signal can be intercepted from a further distance, meaning the aircraft can fly further away from the ground station.

Comparing the computer simulations with the measured values of the built antenna, it can be seen that the real antenna actually have better performance than predicted by the computer simulations. The predicted half power beam width was 50°, while the produced antenna have 40°. The computer simulations predicted side lobe levels less than $-18$ dB, which in the real case turned out to be $-23$ dB.

The major difference between the computer simulations and the real antenna was for the bandwidth. Simulations predicted a 35 MHz bandwidth centered at 2.46 GHz for a VSWR lower than 1.5 and a axial ratio lower than 3 dB, while measurments showed that the real antenna had a bandwidth of 80 MHz centered at 2.44 GHz. No good explation for this difference have been found. It is possible that the fact that the simulations are based on an infinite ground plane, which for obvious reasons not are used in the real design can explain some of the difference. However it is very unlikely that this alone would cause such a big difference in bandwidth.

## 6.1 Future Work

In Section 5.3 it was decided that the spacing between the elements should be $0.6\lambda$, despite the fact that this would give rise to side lobe levels. In order to avoid these side lobe levels the spacing can be reduced to $0.5\lambda$, but at the same time this would lead to increased mutual coupling.

One way of decreasing the spacing and still be able to maintain a distance big enough between the element edges would be to decrease the actual size of each element. This can, for example, be done with the element design given in [22]. An attempt to simulate this element design has been done, but for one reason or another Ensemble was not able to correctly simulate this. Due to that fact this design have not been further investigated in this thesis.

A secondary goal with this thesis, if time permitted, was to design the antenna so that tracking of the aircraft would be possible. Theory for a method called monopulse tracking is described in Section 4.3. It should be possible to redesign the antenna built in this thesis for monopulse tracking capabilities using the feed network described in [23]. This design would require that four hybrids are incorporated in the feed network.

With the help of a phase detector(for example [16]) and ideas presented in section 5.1, it should be possible to design a phased array with similar characteristics as the switched system that the antenna designed in this project is supposed to be used in. With a phased array design, better control of the radiation pattern can be achieved with the ability to position the main beam right on the transmitter and null out any other transmitters. The main

problem with this design should be the signal processing and not the actual antenna design.

# Bibliography


[1] W. L. Stutzman. *Antennna Theory and Design*. John Wiley & Sons, inc., second edition, 1998.

[2] R. A. Sainati. *CAD of Microstrip Antennas for Wireless Applications*. Artech House, Inc., 1996.

[3] N. Andersson, S. Sandberg. Aerosonde Tracking Using a Smart Antenna System. Master's thesis, Lulea University of Technology, 2002.

[4] A. Karlsson. Improvements of Antennas for Areosond Aircraft. Master's thesis, Lulea University of Technology, 2002.

[5] C. A. Balanis. *Advanced Engineering Electromagnetics*. John Wiley & Sons, inc., 1989.

[6] C. A. Balanis. *Antenna Theory: Analysis and Design*. John Wiley & Sons, inc., second edition, 1996.

[7] J. R. James. *Handbook of Microstrip Antennas*. Peter Peregrinus Ltd., 1989.

[8] D. H. Schaubert. Microstrip antennas. *Electromagnetics*, 12(3–4):381–401, July–December 1992.

[9] J. Q. Howell. Microstrip antennas. *IEEE Transactions on Antennas & Propagation*, AP-23(1):90–3, January 1975.

[10] K. R. Carver. Microstrip antenna technology. *IEEE Transactions on Antennas & Propagation*, AP-29(1):2–24, January 1981.

[11] R. J. Mailloux. Microstrip array technology. *IEEE Transactions on Antennas & Propagation*, AP-29(1):25–37, January 1981.

[12] J. D. Kraus. *Antennas*. McGraw–Hill, Inc., second edition, 1988.

[13] L. Rade. *Mathematics Handbook for Science and Engineering: BETA*. Studentlitteratur, third edition, 1995.

[14] D. R. Jackson. Simple approximate formulas for input resistance, bandwidth, and efficiency of a resonant rectagular patch. *IEEE Transactions on Antennas & Propagation*, 39(3):407–10, March 1991.

[15] International Engineering Consortium. http://www.iec.org/online/ tutorials/smart_ant/, 13 December 2001.

[16] 2.7GHz RF / IF Gain Phase Detector. http://products.analog.com/ products/info.asp?product=AD8302, 13 December 2001.

[17] J. C. Liberti, Jr. *Smart Antennas for Wireless Communications : Is-95 and Third Generation Cdma Applications*. Prentice Hall PTR, 1999.

[18] R. P. Jedlicka. Measured mutual coupling between microstrip antennas. *IEEE Transactions on Antennas & Propagation*, Ap-29(1):147–49, January 1981.

[19] H. Pues. Accurate transmission–line model for the rectangular microstrip antenna. *IEE Proceedings*, 131(6):334–40, December 1984.

[20] TLY-5A Data sheet. http://www.taconic-add.com/tlymetric.pdf, 29 December 2001.

[21] ENSEMBLE Design, Review, & 1D Array Synthesis: User's Guide. Version 4.02, February 1996.

[22] W Chen. Inset–microstripline–fed circularly polarized microstrip antennas. *IEEE Antennas and Propagation Society International Symposium. 1999 Digest. Held in conjunction with: USNC/URSI National Radio Science Meeting*, 1:260–3, 1999.

[23] C. M. Jackson. Low cost, $k_a$– band microstrip patch monopulse antenna. *Microwave Journal*, 30(7):125–31, July 1987.

# Appendix A

# Datasheet:TLY

# TLY

## Dimensionally Stable
## Low Loss
## Low Moisture Absorption
## High Peel Strength
## Uniform & Consistent Dk


TACONIC

Mullingar Business Park
Mullingar, Co. Westmeath,
Republic of Ireland
TEL: +353-44-40477
FAX: +353-44-44369

P.O. Box 69 • 136 Coonbrook Road
Petersburgh, NY 12138
TEL: 518-658-3202 • FAX: 518-658-3988
TOLL FREE: 800-833-1805 • FAX: 800-272-2503

302 E-Dong Bundang Techno Park
151Yatap-dong Bundang-gu
Sungnam-si, Kyungki-do
Republic of Korea
TEL: 82-31-704-1858/9
FAX: 82-31-704-1857

# TLY

## APPLICATIONS

Automotive Radars

Satellite Communications

Cellular Communications

Power Amplifiers

LNBs, LNAs, LNCs

Aerospace:

*Radars*
*Guidance Telemetry*
*High Frequency Communication*
*Military*

Taconic has over 35 years of experience coating fiberglass fabric with PTFE (polytetrafluoroethylene). This enables Taconic to manufacture copper clad PTFE/woven glass laminates with exceptionally well controlled electrical and mechanical properties.

Taconic TLY laminates are manufactured from woven fiberglass fabric coated wIth PTFE interleaved with thin sheets of pure PTFE. The woven matrix produces a more mechanically stable laminate with a more uniform dielectric constant (Dk) than traditional non-woven products. The exceptionally low dissipation factor extends the usefulness of this product to 35 GHz and above.

The dielectric constant range is 2.17 to 2.40. For most thicknesses, the dielectric constant can be specified anywhere within this range with a tolerance of ±.02. In the low dielectric constant range, the dissipation factor is approximately 0.0009 when measured at 10 GHz.

TLY laminates can be sheared, drilled, milled and plated using the accepted methods for PTFE/woven fiberglass laminates. The laminates are dimensionally stable and are resistant to the solvents and reagents used during fabrication. TLY laminates are being used in composite multi-layer circuitboard applications.

Typical applications for TLY laminates include mobile communications systems, microwave transmission devices, phased array antennas, RF components, and automotive and military radars.

TLY laminates are generally ordered clad on one or both sides with 1/2, 1, and 2 oz. electrodeposited copper. Contact our Customer Service Department for alternate claddings.

TLY laminates are tested in accordance with IPC-TM 650. A certificate of compliance containing lot-specific test data accompanies each shipment.

See "How to Order" on back page for a complete product listing.

## TLY-5A TYPICAL VALUES

| Property | Test Method | Units | Value | Units | Value |
|---|---|---|---|---|---|
| Dielectric Constant @ 10 GHz | IPC-TM 650 2.5.5.5 | | 2.17 | | 2.17 |
| Dissipation Factor @ 10 GHz | IPC-TM 650 2.5.5.5 | | 0.0009 | | 0.0009 |
| Moisture Absorption | IPC-TM 650 2.6.2.1 | % | <.02 | % | <.02 |
| Dielectric Breakdown | IPC-TM 650 2.5.6 | kV | >60 | kV | >60 |
| Volume Resistivity | IPC-TM 650 2.5.17.1 | Mohm/cm | $10^7$ | Mohm/cm | $10^7$ |
| Surface Resistivity | IPC-TM 650 2.5.17.1 | Mohm | $10^7$ | Mohm | $10^7$ |
| Arc Resistance | IPC-TM 650 2.5.1 | seconds | >180 | seconds | >180 |
| Flexural Strength Lengthwise | IPC-TM 650 2.4.4 | lbs./in. | >12,000 | N/mm$^2$ | >83 |
| Flexural Strength Crosswise | IPC-TM 650 2.4.4 | lbs./in. | >10,000 | N/mm$^2$ | >69 |
| Peel Strength (1oz copper) | IPC-TM 650 2.4.8 | lbs./linear in. | 12.0 | N/mm | 2.1 |
| Thermal Conductivity | Cenco-Fitch | BTU/in./hr/ft$^2$/°F | 2.79 | W/m/K | 0.40 |
| x-y CTE | ASTM D 3386 (TMA) | ppm/°C | 20 | ppm/°C | 20 |
| z CTE | ASTM D 3386 (TMA) | ppm/°C | 280 | ppm/°C | 280 |
| UL-94 Flammability Rating | UL-94 | | V-0 | | V-0 |

| Type | | Dk |
|---|---|---|
| TLY-5A | | 2.17 |
| TLY-5 | | 2.20 |
| TLY-3 | | 2.33 |
| TLT-0 | TLX-0 | 2.45 |
| TLT-9 | TLX-9 | 2.50 |
| TLT-8 | TLX-8 | 2.55 |
| TLT-7 | TLX-7 | 2.60 |
| TLT-6 | TLX-6 | 2.65 |
| TLE-95 | | 2.95 |
| TLC-27 | | 2.75 |
| TLC-30 | | 3.00 |
| TLC-32 | | 3.20 |
| RF-30 | | 3.00 |
| RF-35 | | 3.50 |
| RF-60 | | 6.15 |
| CER-10 | | 10 |

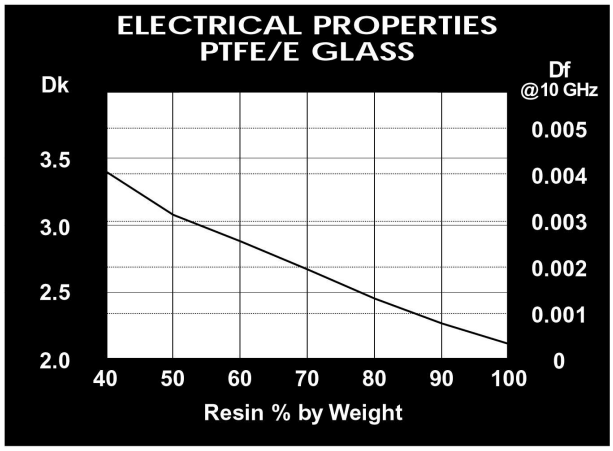


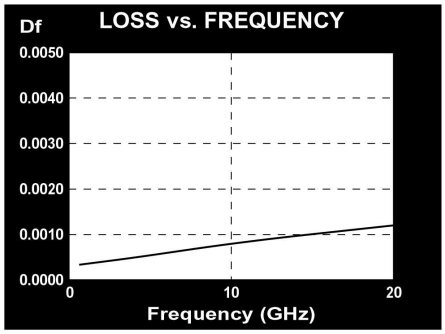


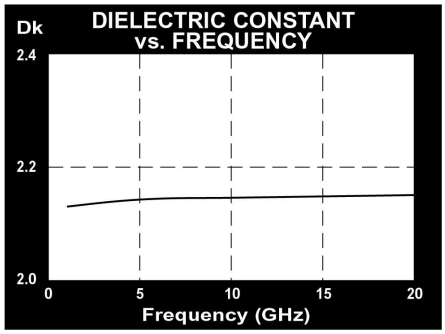


2/01

# How to Order

| Designation | Dielectric Constant | Dielectric Thickness | Dielectric Thickness |
|---|---|---|---|
| TLY - 5A | 2.17 +/– .02 | ≥ .0310" | ≥ 0.80mm |
| TLY - 5 | 2.20 +/– .02 | ≥ .0050" | ≥ 0.13mm |
| TLY - 3 | 2.33 +/– .02 | ≥ .0050" | ≥ 0.13mm |

*Standard sheet size is 36" x 48" (914mm x 1220mm). Please contact our Customer Service Department for the availability of other sizes and claddings.*

TLY can be ordered with the following electrodeposited copper:

| Designation | Weight | Copper Thickness | Copper Thickness |
|---|---|---|---|
| CH | 1/2 oz./sq. ft. | ~ .0007" | ~18 μm |
| C1 | 1 oz./sq. ft. | ~ .0014" | ~ 35 μm |
| C2 | 2 oz./sq. ft. | ~ .0028" | ~ 70 μm |

Panels may be ordered cut to size

| Typical Panel Sizes | |
|---|---|
| 12" x 18" | 304mm x 457mm |
| 16" x 18" | 406mm x 457mm |
| 18" x 24" | 457mm x 610mm |
| 16" x 36" | 406mm x 914mm |
| 24" x 36" | 610mm x 914mm |
| 18" x 48" | 457mm x 1220mm |

**An example of our part number is: TLY-5-0100-CH/CH-18" x 24" (TLY-5-0100-CH/CH-457mm x 610mm)**

TACONIC
ADVANCED DIELECTRIC DIVISION

P.O. Box 69 • 136 Coonbrook Road
Petersburgh, New York 12138 • USA
TEL: 518-658-3202 • FAX: 518-658-3988
TOLL FREE: 800-833-1805 • FAX: 800-272-2503

Mullingar Business Park
Mullingar, Co. Westmeath,
Republic of Ireland
TEL: +353-44-40477 • FAX: +353-44-44369

302 E-Dong Bundang Techno Park
151 Yatap-dong Bundang-gu
Sungnam-si, Kyungki-do, Republic of Korea
TEL: 82-31-704-1858/9 • FAX: 82-31-704-1857